Joint parameter optimization of differentiated discretization schemes for audio circuits

Audio Engineering Society

Convention Paper 9751

Presented at the 142nd Convention
2017 May 20–23, Berlin, Germany

Joint parameter optimization of differentiated discretization schemes for audio circuits

François G. Germain[1] and Kurt James Werner[2]

[1]*Center for Computer Research in Music and Acoustic (CCRMA), Stanford University, Stanford, CA, United States*
[2]*Sonic Arts Research Centre (SARC), Queen's University Belfast, Belfast, United Kingdom*

Correspondence should be addressed to François G. Germain (francois@ccrma.stanford.edu)

ABSTRACT

We propose a new approach to discretizing audio circuits which involves applying differentiated discretization schemes among the elements of a linear circuit, or sub-circuit, rather than a single uniform scheme. The scheme coefficients are jointly optimized to minimize some frequency response error function for that linear circuit. We describe the mathematical framework for this optimization and apply it to the case of the parametric bilinear transform. Differentiated discretization coefficients are jointly optimized by minimizing the L^2-norm error between the discretized frequency response and the frequency response of the original system. To demonstrate the validity of our approach, we apply our method to several examples and show a systematic reduction of the frequency response error in each case.

1 Introduction

Computational modeling of audio systems (i.e., virtual analog modeling) is a major topic of interest, including emulation of existing electronic and acoustic systems such as vintage audio effects or acoustic instruments. This main goal of this modeling process is the design of discrete-time systems emulating the behavior of a target continuous-time system. When the exact dynamics of that system are known through a set of differential equations, a common procedure is to discretize it using a discretization schemes [1, 2, 3]. In our particular case of interest where the system is linear time-invariant (LTI), additional techniques are available using a filter design approach, through the use of various s-to-z mapping methods [4, 5], pole/zero mapping methods [6, 7], and frequency response optimization methods [8, 9].

Those methods have a variety of advantages and drawbacks. Discretization schemes in particular are generally designed following concepts such as order of accuracy and stability and can be applied systematically to the system equations. These properties guarantee the versatility of those methods for consistently generating discrete-time models from any system whose equations are known with some guaranteed level of accuracy.

One popular discretization scheme approach in the virtual analog field is the standard bilinear transform [10]. It is typically used in common methods for structuring discrete-time models, such as the state-space approach [11, 12], and the wave digital filter approach [13, 14]. While it is limited in accuracy due to its simplicity, it has been historically favored in the audio field as it preserves the system order while providing the highest possible degree of accuracy, allowing for compact system representation and efficient computation. It also has the property of unconditionally preserving stability

and minimum-phase properties [3, 10]. This proves useful as digital audio effects typically work with a prescribed sampling frequency. One well-known response distortion of the method is the frequency warping of the system frequency response [15]. However, the transform belongs to a wider class of methods based on Möbius transforms [16] (along with the Euler methods), whose coefficients can be altered while preserving some of their desirable properties. In particular, in the case where the frequency response is characterized by a salient feature located at a single frequency, we can alter a single coefficient of the bilinear transform to form the so-called "parametric bilinear transform" and ensure that the response at the salient feature frequency is matched between the original system and its discretized version. However, as this approach can solely match a single frequency, it behaves poorly when the response exhibits two or more salient features spread in frequency [17].

Discretization methods like the bilinear transform have limited opportunity for tuning. Some classes of methods do however present some free parameters, and optimization approaches exist [18, 19, 20]. This optimization is however either done on the general scheme, optimizing generic properties such as dissipation or dispersion, or it is limited to a particular differential equation, such as the wave equation. Additionally, those approaches generally target distributed systems (i.e., partial difference equations) rather than lumped systems (i.e., ordinary difference equations) which are very common in virtual analog research. Optimization has also been leveraged to alleviate additional sources of modeling error, such as inaccurate component values [21]. A recent paper [16] introduced an approach to optimize discretization schemes based on Möbius transforms for lumped systems in order to improve transient behavior of the discretized system while preserving stability. Another approach [22] showed how we can minimize the time domain simulation error in a Wave Digital Filter simulation through an appropriate Möbius transform parametrization.

In a lot of cases, we have a modular knowledge of the physical system of interest. That system is thus composed of a network of known elements with their individual equations. When using discretization schemes, it is then equivalent to apply the method at once to the general equation systems, or to apply it individually to each of those elements and then combine them into a global discretized system. The schemes are however generally applied identically to each of these elements.

In this paper, we introduce the possibility of differentiating the discretization schemes among the different elements of the circuit in order to greatly increase the degrees of freedom available to tune and ultimately improve the behavior of the discretized system, i.e., improve the match between the frequency response of the original system and its discretized version across a wide frequency region. By maintaining the usage of some form of bilinear transform across the entire circuit, we conserve the desirable properties attached to the scheme. This also has the advantage of not requiring any explicit derivation of the poles and/or zero of that system, which is sometimes required for other types of methods (e.g., pole/zero mapping). For our proof of concept, we limit the present analysis to linear circuits or sub-circuits with a single open free port which can be plugged into a larger system.

In Sec. 2, we introduce the mathematical description of the different circuit systems under consideration in the continuous- and discrete-time domains. In Sec. 3, we present our discretization approach and the coefficient selection optimization procedure. In Sec. 4, we apply those principles to the discretization of simple examples to demonstrate the frequency response improvement of our approach over typical approaches using the standard and the parametric bilinear transforms.

1.1 Notation

Bolded uppercase letters ($\mathbf{A}, \mathbf{B}, \mathbf{C}, \ldots$) denote matrices, and bolded lowercase letters ($\boldsymbol{a}, \boldsymbol{b}, \boldsymbol{c}, \ldots$) denote (column) vectors. We denote row vectors as transposed column vectors. $\mathbf{I}_p$ denotes the identity matrix of size $p \times p$. $\mathbf{0}_p$ denotes the zero (column) vector of length p. $\mathbf{0}_{p,q}$ denotes the zero matrix of size $p \times q$. Quantities with a hat ($\hat{a}, \hat{\boldsymbol{a}}, \hat{\mathbf{A}}, \ldots$) are used for the discretized system (generally functions of z^{-1}), corresponding to matching quantities for the continuous-time system (and functions of s). * denotes complex conjugation and $^\mathsf{T}$ denotes matrix transposition.

2 System description

2.1 Linear circuits with one free port

In the context of this paper, we focus on circuits formed of independent LTI elements (resistor, capacitor, inductor) with one free port, as defined in classical network

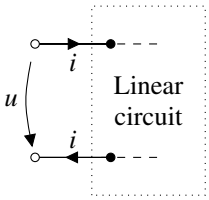

Fig. 1: Linear circuit with one free port.

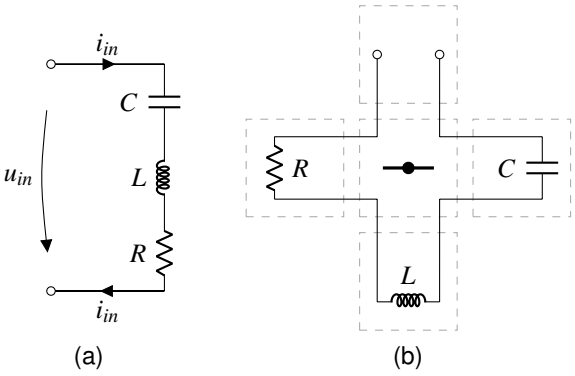

Fig. 2: (a) RLC series circuit and (b) equivalent connection tree with one free port.

theory [23]. Fig. 1 shows the general structure of such circuit, and Fig. 2 shows a simple example. The free port is considered as a driving port, and it is characterized by a pair of input–output variables. Those variables are typically chosen among the Kirchhoff variables (voltage and current) or linear transformations of those variables (e.g., wave variables [24]).

To form the complete circuit analysis, we need to characterize the quantities at the free driving port. We define the input variable as a linear combination of the port branch voltage u_e and branch current i_e as $e = \alpha i_e - \beta u_e$. We then form an added input branch plugged at the free driving port that emulates that input variable e, hence "closing" the free port with an equivalent "source" element. The desired output o can then be measured as another linear combination $o = \gamma i_e - \delta u_e$.

Typical input–output combinations are described by:

- voltage–current: $\beta = \gamma = 1$ and $\alpha = \delta = 0$;
- current–voltage: $\beta = \gamma = 0$ and $\alpha = \delta = 1$;
- incident–reflected voltage waves for a port resistance R: $\beta = \delta = -1$ and $\alpha = -\gamma = R$;

2.2 Tableau formulation

Tableau formulation is a standard circuit analysis technique [25], representing the circuit equations relating the circuit node voltages $\boldsymbol{v}$, branch voltages $\boldsymbol{u}$ and branch currents $\boldsymbol{i}$ through the Kirchhoff voltage law equations

$$\boldsymbol{u} - \mathbf{A}^\mathsf{T}\boldsymbol{v} = \mathbf{0}_b, \tag{1}$$

the Kirchhoff current law equations

$$\mathbf{A}\boldsymbol{i} = \mathbf{0}_n, \tag{2}$$

and the (linear) branch equations

$$\mathbf{K}\boldsymbol{u} + \mathbf{Z}\boldsymbol{i} = \boldsymbol{w}. \tag{3}$$

$\mathbf{A}$ is the reduced incidence matrix of the circuit, with its coefficients being only -1, 0 and 1. $\boldsymbol{w}$ is the source vector. $\mathbf{K}$ and $\mathbf{Z}$ correspond to the coefficients forming the branch equations expressed in the Laplace domain for LTI circuits. Since all the considered circuit elements are independent, $\mathbf{K}$ and $\mathbf{Z}$ are diagonal.

The full system is then represented as:

$$\begin{bmatrix} \mathbf{I}_b & \mathbf{0}_{b,b} & -\mathbf{A}^\mathsf{T} \\ \mathbf{K} & \mathbf{Z} & \mathbf{0}_{b,n} \\ \mathbf{0}_{n,b} & \mathbf{A} & \mathbf{0}_{n,n} \end{bmatrix} \begin{bmatrix} \boldsymbol{u} \\ \boldsymbol{i} \\ \boldsymbol{v} \end{bmatrix} = \begin{bmatrix} \mathbf{0}_b \\ \boldsymbol{w} \\ \mathbf{0}_n \end{bmatrix} \tag{4}$$

In Tableau formulation, we set one node voltage as datum node (i.e., force this node to 0) and remove it from the node voltage variable list. The resulting system variables are then uniquely determined, i.e. the system is invertible.

Through Eq. (1), it is well-known we can eliminate the branch voltage variables to form the system [25]:

$$\begin{bmatrix} \mathbf{Z} & \mathbf{K}\mathbf{A}^\mathsf{T} \\ \mathbf{A} & \mathbf{0}_{n,n} \end{bmatrix} \begin{bmatrix} \boldsymbol{i} \\ \boldsymbol{v} \end{bmatrix} = \begin{bmatrix} \boldsymbol{w} \\ \mathbf{0}_n \end{bmatrix} \tag{5}$$

with only branch currents and node voltages as unknowns.

2.3 Branch equations

As our circuit is composed by independent LTI elements, the branch equations we obtain are well-known in the Laplace domain. We take as a convention that the coefficients z of matrix $\mathbf{Z}$ match the impedances of the corresponding elements. Independent LTI elements are of three kinds:

- resistors with resistance R:

$$u_R - Ri_R = 0 \tag{6}$$

  i.e. $z_R(s) = \frac{1}{y_R(s)} = R$, $k_R = -1$, and $w_R = 0$;

- inductors with inductance L:

$$u_L - sLi_L = 0 \tag{7}$$

  i.e. $z_L(s) = \frac{1}{y_L(s)} = sL$, $k_L = -1$, and $w_L = 0$;

- capacitors with capacitance C:

$$u_C - i_C/(sC) = 0 \tag{8}$$

  i.e. $z_C(s) = \frac{1}{y_C(s)} = (sC)^{-1}$, $k_C = -1$, and $w_C = 0$;

Using this convention, we notice that all the coefficients k for those elements are equal to -1, while all the w coefficients are 0. We can then collect all the z coefficients of those linear elements in a diagonal matrix $\mathbf{Z}_l$ (denoted "impedance" matrix as the z coefficients correspond to the impedances of each element), all the k coefficients in a diagonal matrix $\mathbf{K}_l = -\mathbf{I}_l$, and all the w coefficients in the zero vector $\boldsymbol{w}_l = \mathbf{0}_l$.

The remaining branch equation corresponds to the input branch at the driving port:

$$\alpha i_e - \beta u_e = e \tag{9}$$

i.e. $z_e = \alpha$, $k_e = -\beta$, and $w_e = e$.

We can then partition and simplify Eq. (5) into:

$$\begin{bmatrix} \mathbf{Z}_l & \mathbf{0}_l & -\mathbf{A}_l^\mathsf{T} \\ \mathbf{0}_l^\mathsf{T} & \alpha & -\beta \boldsymbol{a}_e^\mathsf{T} \\ \mathbf{A}_l & \boldsymbol{a}_e & \mathbf{0}_{n,n} \end{bmatrix} \begin{bmatrix} \boldsymbol{i}_l \\ i_e \\ \boldsymbol{v} \end{bmatrix} = \begin{bmatrix} \mathbf{0}_l \\ e \\ \mathbf{0}_n \end{bmatrix} = e \begin{bmatrix} \mathbf{0}_l \\ 1 \\ \mathbf{0}_n \end{bmatrix} \tag{10}$$

2.4 System transfer function

As we pointed out earlier, this system is invertible, so that we can compute the solution for all the branch current and node voltages as:

$$\begin{bmatrix} \boldsymbol{i}_l \\ i_e \\ \boldsymbol{v} \end{bmatrix} = e \begin{bmatrix} \mathbf{Z}_l & \mathbf{0}_l & -\mathbf{A}_l^\mathsf{T} \\ \mathbf{0}_l^\mathsf{T} & \alpha & -\beta \boldsymbol{a}_e^\mathsf{T} \\ \mathbf{A}_l & \boldsymbol{a}_e & \mathbf{0}_{n,n} \end{bmatrix}^{-1} \begin{bmatrix} \mathbf{0}_l \\ 1 \\ \mathbf{0}_n \end{bmatrix} \tag{11}$$

On the other hand, the output quantity is expressed as:

$$o = \gamma i_e - \delta u_e = \begin{bmatrix} \mathbf{0}_l \\ \gamma \\ -\delta \boldsymbol{a}_e \end{bmatrix}^\mathsf{T} \begin{bmatrix} \boldsymbol{i}_l \\ i_e \\ \boldsymbol{v} \end{bmatrix} \tag{12}$$

so that the system transfer function $H(s) = o/e$ is expressed as:

$$H(s) = \begin{bmatrix} \mathbf{0}_l \\ \gamma \\ -\delta \boldsymbol{a}_e \end{bmatrix}^\mathsf{T} \begin{bmatrix} \mathbf{Z}_l & \mathbf{0}_l & -\mathbf{A}_l^\mathsf{T} \\ \mathbf{0}_l^\mathsf{T} & \alpha & -\beta \boldsymbol{a}_e^\mathsf{T} \\ \mathbf{A}_l & \boldsymbol{a}_e & \mathbf{0}_{n,n} \end{bmatrix}^{-1} \begin{bmatrix} \mathbf{0}_l \\ 1 \\ \mathbf{0}_n \end{bmatrix} \tag{13}$$

Using inversion by block formulas [26] and assuming $s \neq 0$ (so that $\mathbf{Z}_l$ is invertible), we finally get that:

$$H(s) = \frac{\gamma + \delta \boldsymbol{a}_e^\mathsf{T} (\mathbf{A}_l \mathbf{Y}_l \mathbf{A}_l^\mathsf{T})^{-1} \boldsymbol{a}_e}{\alpha + \beta \boldsymbol{a}_e^\mathsf{T} (\mathbf{A}_l \mathbf{Y}_l \mathbf{A}_l^\mathsf{T})^{-1} \boldsymbol{a}_e} \tag{14}$$

where $\mathbf{Y}_l = \mathbf{Z}_l^{-1}$ is the "admittance" diagonal matrix whose diagonal terms are the admittances of the linear elements of the system. For conciseness of notation, we denote $\boldsymbol{\Phi} = \mathbf{A}_l \mathbf{Y}_l \mathbf{A}_l^\mathsf{T}$, and $\theta = \boldsymbol{a}_e^\mathsf{T} \boldsymbol{\Phi}^{-1} \boldsymbol{a}_e$ so that:

$$H(s) = \frac{\gamma + \delta \boldsymbol{a}_e^\mathsf{T} \boldsymbol{\Phi}^{-1} \boldsymbol{a}_e}{\alpha + \beta \boldsymbol{a}_e^\mathsf{T} \boldsymbol{\Phi}^{-1} \boldsymbol{a}_e} = \frac{\gamma + \delta \theta}{\alpha + \beta \theta} \tag{15}$$

Then, for typical input–output combinations, we can express the system transfer function as follows:

- voltage–current: $H(s) = 1/\theta$;
- current–voltage: $H(s) = \theta$;
- incident–reflected voltage waves for a port resistance R: $H(s) = (\theta + R)/(\theta - R)$.

3 System discretization

Simulating a system in continuous time is generally impractical if not intractable. The discretization of the system aims at constructing an equivalent tractable system where the system variables are computed at discrete time steps. For LTI systems whose behavior can be expressed as a transfer function in the s-plane $H(s)$, the corresponding discretized system can be expressed as a transfer function in the z-plane $\hat{H}(z^{-1})$. We denote the complex frequency response of the continuous-time system at radian frequency Ω as $H(j\Omega)$, and the one of the discretized system is given by $\hat{H}(e^{-j\Omega T})$.

3.1 Error description

Discretization generally introduces some error in the system frequency response. Denoting $H_\Omega = H(j\Omega)$ and $\hat{H}_\Omega = \hat{H}(e^{-j\Omega T})$, we describe the error ε introduced by the system as the L^2-norm of the frequency response error of the system on the radian frequency range $[\Omega_{\min}, \Omega_{\max}] \subset [0, \pi/T]$:

$$\varepsilon = \int_{\Omega_{\min}}^{\Omega_{\max}} |H_\Omega - \hat{H}_\Omega|^2 d\Omega \tag{16}$$

Note that, in general, we have no guarantee that ε will be convex as a function of the discretization parameters.

3.2 Discretized transfer function

Typical discretization schemes (e.g., Euler methods, bilinear transform) used to discretize the system transfer function can be equivalently applied to the complete transfer function $H(s)$ to obtain $\hat{H}(z^{-1})$, or applied individually to each element of the circuit. For the latter, we alter the branch equations, substituting the discretized versions $\hat{z}_R$, $\hat{z}_C$, $\hat{z}_L$ of z_R, z_C, z_L. Applying that substitution to all M linear elements in the system, we get their respective impedance $\hat{z}_m$ and admittance $\hat{y}_m$ ($m \in \{1 \dots M\}$) and form the diagonal matrices $\hat{\mathbf{Z}}_l$ and $\hat{\mathbf{Y}}_l$ to compute the discretized transfer function as:

$$\hat{H}(z^{-1}) = \frac{\gamma + \delta \boldsymbol{a}_e^\mathsf{T} (\mathbf{A}_l \hat{\mathbf{Y}}_l \mathbf{A}_l^\mathsf{T})^{-1} \boldsymbol{a}_e}{\alpha + \beta \boldsymbol{a}_e^\mathsf{T} (\mathbf{A}_l \hat{\mathbf{Y}}_l \mathbf{A}_l^\mathsf{T})^{-1} \boldsymbol{a}_e} = \frac{\gamma + \delta \hat{\theta}}{\alpha + \beta \hat{\theta}} \tag{17}$$

From Eqs. (15) and (17), the error from (16) becomes:

$$\varepsilon = \int_{\Omega_{\min}}^{\Omega_{\max}} \left| \frac{(\alpha\delta - \gamma\beta)(\hat{\theta} - \theta)}{(\alpha + \beta\theta)\left(\alpha + \beta\hat{\theta}\right)} \right|^2 d\Omega \tag{18}$$

3.3 Error minimization

In the case where the discretization has a free parameter ϕ, we can minimize the error as a function of that parameter by solving the optimization problem:

$$\phi_{\min} = \arg\min_\phi \, \varepsilon(\phi) \tag{19}$$

We cannot typically solve this problem analytically, but it is suitable for numerical optimization algorithms using the analytical error function gradient. As only the admittances $\hat{y}_m$ depend on the discretization method, the partial derivative of the error function with respect to ϕ is:

$$\frac{\partial \varepsilon}{\partial \phi} = 2\Re \left[\int_{\Omega_{\min}}^{\Omega_{\max}} \frac{(\alpha\delta - \gamma\beta)^2 (\hat{\theta}^* - \theta^*) \frac{\partial \hat{\theta}}{\partial \phi} d\Omega}{(\alpha + \beta\theta^*)|\alpha + \beta\hat{\theta}|^2 (\alpha + \beta\hat{\theta})} \right] \tag{20}$$

with:

$$\frac{\partial \hat{\theta}}{\partial \phi} = -\sum_{m=1}^{M} (\boldsymbol{a}_e^\mathsf{T} \hat{\boldsymbol{\Phi}}^{-1} \boldsymbol{a}_m)^2 \frac{\partial \hat{y}_m}{\partial \phi} \tag{21}$$

3.4 Parametric bilinear transform

One of the most common discretization methods in the context of virtual analog research is the standard bilinear transform, which corresponds to the trapezoidal rule in numerical integration [16]. For an LTI system, the discretized transfer function can be obtained from the continuous-time transfer function expressed in the Laplace domain by replacing each instance of the Laplace s variable by a function of z^{-1} [16] following the mapping:

$$s \mapsto \frac{2}{T} \frac{1 - z^{-1}}{1 + z^{-1}} \tag{22}$$

where T refers to the sampling period of the discretized system. A well-known distortion introduced by this method is the so-called "frequency warping". While ideally, we would like the original and discretized systems to have identical responses at each frequency (i.e., $H(j\Omega) = \hat{H}(e^{-j\Omega T})$ for all $\Omega \in [-\pi/T, \pi/T]$), the system obtained using the standard bilinear transform verifies instead $H(j\Omega) = \hat{H}(e^{-j\omega T})$ with the "warping" relation:

$$\omega = \frac{2}{T} \tan^{-1}\left(\frac{\Omega T}{2}\right) \tag{23}$$

The parametric bilinear transform is a common way to modify the standard bilinear transform in order to alter the warping distortion [15]. By replacing the quantity T in Eq. (22) with an appropriately chosen coefficient T', we can enforce the property that $H(j\Omega) = \hat{H}(e^{-j\Omega T})$ for a *single* "matched" radian frequency Ω using:

$$T' = \frac{2}{\Omega} \tan\left(\frac{\Omega T}{2}\right) \tag{24}$$

Note that we have the relation $T' = T + O(T^2)$, meaning all parametric bilinear transforms preserve the property of the standard transform of being second-order accurate and unconditionally stable.

The resulting system then exhibits a different frequency warping, as $H(j\Omega) = \hat{H}(e^{-j\omega' T})$ for:

$$\omega' = \frac{2}{T'} \tan^{-1}\left(\frac{\Omega T}{2}\right) \tag{25}$$

The matched radian frequency is typically chosen to match the frequency of a salient property of the original system frequency response (e.g., resonant frequency, cutoff frequency) in the discretized system frequency response. However, only a single frequency can be matched, leaving no additional control over the error at other frequencies. This can become problematic if the system frequency response exhibits salient features spread over a wide frequency range [17].

With T' as free parameter, we can complete the gradient expression in Eq. (21) with:

$$\frac{\partial \hat{y}_m}{\partial T'} = \begin{cases} 0 & \text{for resistors} \\ \frac{1}{2L_m} \frac{1+z^{-1}}{1-z^{-1}} & \text{for inductors} \\ \frac{2C_m}{T'^2} \frac{z^{-1}-1}{z^{-1}+1} & \text{for capacitors} \end{cases} \tag{26}$$

3.5 Differentiated discretization

In typical applications, the bilinear transform (standard or parametric) is applied globally to the system, resulting in the frequency distortion outlined in Sec. 3.4. Our approach here is to instead apply a different parametric bilinear transform to each linear element in the circuit.

By construction, the coefficients of the branch equations (associated with the M linear elements of the circuits) are distributed on the diagonal of $\mathbf{Z}$. The mth diagonal coefficient then contains at most one instance of s that we "attach" to that coefficient (and denote s_m). Applying differentiated transforms to each element then corresponds to selecting M coefficients T'_m ($m \in \{1 \dots M\}$) so that we form the matrices $\hat{\mathbf{Z}}_l$ and $\hat{\mathbf{Y}}_l$ by mapping any instance of s_m (associated with the branch equation of the mth element) as:

$$s_m \mapsto \frac{2}{T'_m} \frac{1-z^{-1}}{1+z^{-1}} \tag{27}$$

In our differentiated discretization, $\hat{y}_m$ depends only on with its associated parameter T'_m so that the partial derivatives in Eq. (21) for $m, n \in \{1 \dots M\}$ become:

$$\frac{\partial \hat{y}_m}{\partial T'_n} = \begin{cases} 0 & \text{for resistors} \\ \frac{1}{2L_m} \frac{1+z^{-1}}{1-z^{-1}} \times \mathbf{1}_{\{m=n\}} & \text{for inductors} \\ \frac{2C_m}{T'^2_m} \frac{z^{-1}-1}{z^{-1}+1} \times \mathbf{1}_{\{m=n\}} & \text{for capacitors} \end{cases} \tag{28}$$

where $\mathbf{1}_{\{m=n\}}$ equals 1 if $m = n$, 0 otherwise. Since the resistor admittance does not depend on s, varying its associated T' has no effect on the transfer function. We can then exclude resistor branches from the optimization for computational efficiency and we also do not need to report an optimized coefficient value for them.

4 Case studies

We apply our approach to two different circuits to validate it. First, we look at a resonant RLC series circuit with a single resonance. Then we look at a Helmholtz resonator tree like the ones presented in [27] which exhibits multiple resonances. In both cases, we look at the frequency response error introduced by the typical standard bilinear transform (*BLT*), the parametric bilinear transform using the same T' coefficient system-wide (*PBLT*), and our approach (*Diff.*) using the jointly optimized differentiated T'_m coefficients among linear circuit elements compared to the response of the original continuous-time system (*Analog*).

4.1 Algorithms

In order to compute the different integral quantities (Eqs. (18) and (20)), we use the MATLAB implementation[1] of the adaptive Simpson quadrature [28]. For the optimization, we use the MATLAB implementation[2] of a subspace trust-region algorithm based on the interior-reflective Newton method from [29], to which we supply the analytic gradient expression from Eq. (20). All the algorithms are applied using the default parameters. All the systems are sampled at 44.1 kHz (or $T = 22.68\,\mu$s). The optimization is performed over the frequency range $[20\,\text{Hz}, 20\,\text{kHz}]$, which represents the frequency range of interest for audio applications. For the initial point of the optimization process, we set all the T'_m coefficients as $T'_m = T$.

4.2 RLC series circuit

We study a resonant RLC series circuit such as the one in Fig. 2, with the lowest node as datum node. For this system, we then have

$$\mathbf{A}_l = \begin{bmatrix} 1 & -1 & 0 \\ 0 & 1 & -1 \\ 0 & 0 & 1 \end{bmatrix}, \quad \boldsymbol{a}_e = \begin{bmatrix} 0 \\ 0 \\ -1 \end{bmatrix}$$

[1] https://www.mathworks.com/help/matlab/ref/quad.html

[2] https://www.mathworks.com/help/optim/ug/fminunc.html

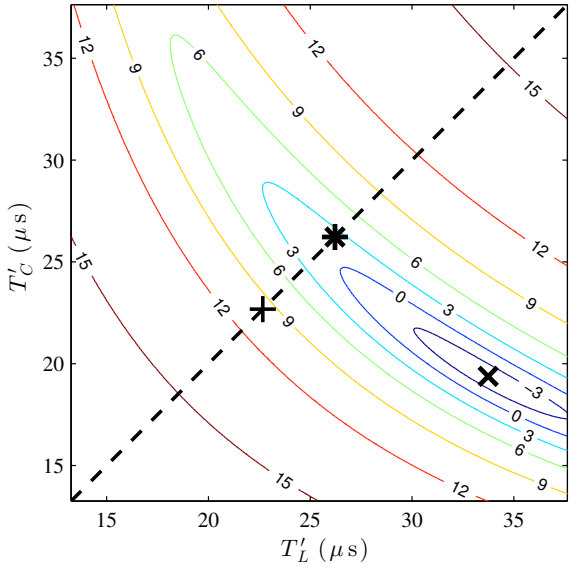

Fig. 3: Contour plot of ε (in dB scale) for an RLC series circuit for the differentiated parametrizations (T'_C, T'_L). Error locations for the different approaches are indicated (BLT: $+$, PBLT: $*$, Diff.: $\times$). The dashed line indicates the space of possible parametrization of the bilinear transforms using a system-wide T' coefficient.

Table 1: Jointly optimized differentiated T' coefficients for the RLC series circuit.

name	value	name	value
T'_C	19.38 µs	T'_L	33.74 µs

$$\text{and } \mathbf{Z}_l = \begin{bmatrix} 1/(sC) & 0 & 0 \\ 0 & sL & 0 \\ 0 & 0 & R \end{bmatrix}. \qquad (29)$$

We optimize the voltage–current transfer function of the system. The parameters are $R = 25\,\Omega$, $L = 2\,\text{mH}$, $C = 0.2\,\mu\text{F}$. As such, the RLC circuit has a resonance at 7.958 kHz, with a quality factor Q of 4. In the case of the parametric bilinear transform, the typical approach is to pick T' to match the frequency response at the resonant peak ($T' = 25.46\,\mu\text{s}$).

The error values ε for various combinations of T'_C and T'_L are shown in Fig. 3. The error locations for the standard bilinear transform, the parametric bilinear transform matching the resonant peak and the jointly optimized differentiated discretization are also indicated.

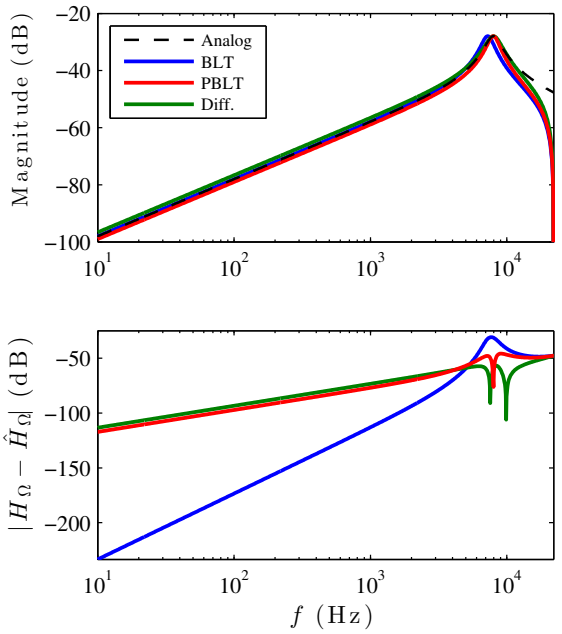

Fig. 4: Magnitude response (top) and error $|H_\Omega - \hat{H}_\Omega|$ (bottom) for different discretization approaches applied to the RLC series circuit.

Table 2: Error ε for different discretization approaches applied to the RLC series circuit.

	BLT	PBLT	Diff.
ε	9.8884	1.2120	0.3448

The plot shows that the standard bilinear transform introduces significant frequency response error compared to the differentiated method. We also see that using any version of the parametric bilinear transform system-wide (i.e., moving along the dashed line) cannot lower the error as much as it can be using clearly differentiated T' coefficients for the capacitor and the inductor. Finally, we see how the heuristic of matching the resonant peak is not exactly equivalent to minimizing the error ε as function of T'.

Tab. 1 shows the T' coefficients found after the joint optimization. Tab. 2 shows how much the differentiated approach lowers the error compared to the standard bilinear transform and the parametric bilinear transform (matching the resonant peak). Figs. 4 and 5 show full-range and zoomed-in frequency responses and error $|H_\Omega - \hat{H}_\Omega|$ for the standard bilinear transform, the

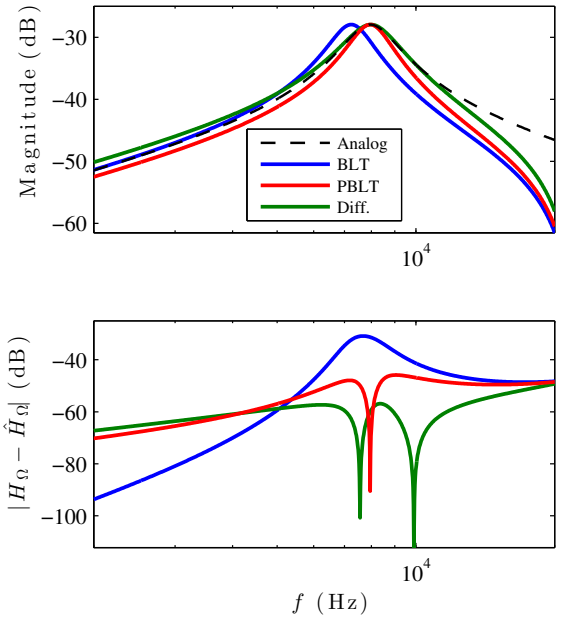

Fig. 5: Zoomed-in magnitude response (top) and error $|H_\Omega - \hat{H}_\Omega|$ (bottom) for different discretization approaches applied to the RLC series circuit.

Table 3: Electrical component values of the Helmholtz resonator tree.

H00		H10		H11	
name	value	name	value	name	value
R_{00}	25 Ω	R_{10}	25 Ω	R_{11}	25 Ω
L_{00}	10 mH	L_{10}	50 mH	L_{11}	250 mH
C_{00}	1 µF	C_{10}	5 µF	C_{11}	25 µF

parametric bilinear transform and the differentiated discretization. For the standard bilinear transform, the frequency warping introduces significant error around the resonant peak. The parametric bilinear transform cancels the error at the peak location but a lot of error remains around it because the peak width of the original system and the discretized system do not match [8]. The jointly optimized differentiated discretization lowers the error, distributes it more uniformly across the frequency range, and matches much better the resonant peak in frequency and width.

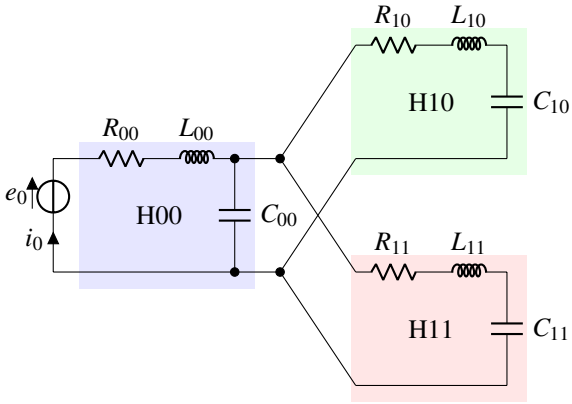

Fig. 6: Helmholtz resonator tree.

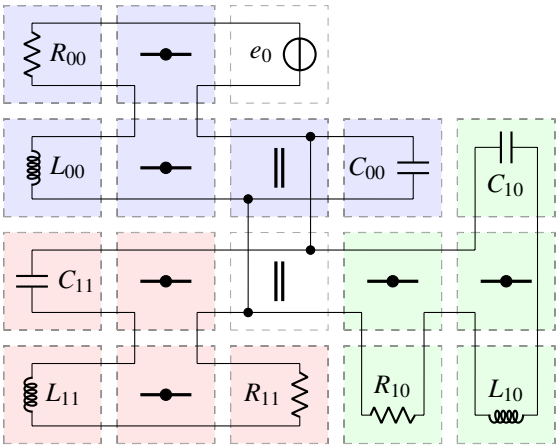

Fig. 7: Helmholtz resonator tree connection tree.

4.3 Helmholtz resonator tree

We then study a Helmholtz resonator tree circuit [27] such as the one in Figs. 6 and 7, with the lower-right node as datum node. For this system, we have

$$\mathbf{A}_l = \begin{bmatrix} 1 & -1 & 0 & 0 & 0 & 0 & 0 \\ 0 & 1 & -1 & 0 & 0 & 0 & 0 \\ 0 & 0 & 1 & 0 & 0 & 0 & 0 \\ 0 & 0 & 1 & -1 & 0 & 0 & 0 \\ 0 & 0 & 0 & 1 & -1 & 0 & 0 \\ 0 & 0 & 0 & 0 & 1 & 0 & 0 \\ 0 & 0 & 1 & 0 & 0 & -1 & 0 \\ 0 & 0 & 0 & 0 & 0 & 1 & -1 \\ 0 & 0 & 0 & 0 & 0 & 0 & 1 \end{bmatrix}^\mathsf{T},$$

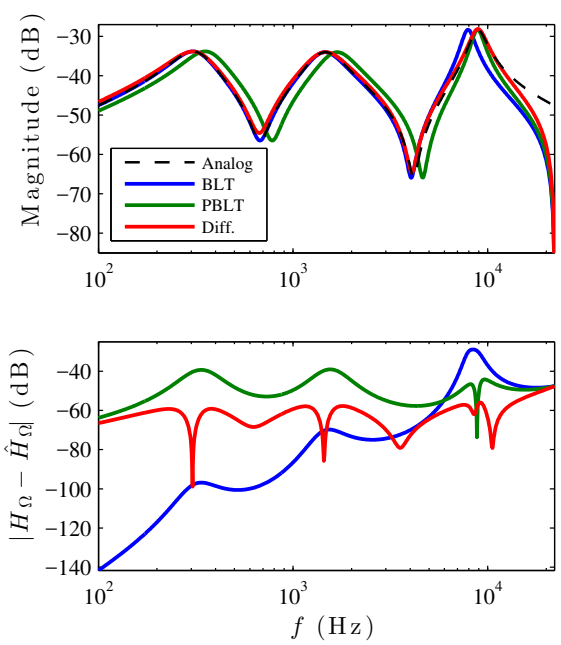

Fig. 8: Magnitude response (top) and error $|H_\Omega - \hat{H}_\Omega|$ (bottom) for different discretization approaches applied to the Helmholtz resonator tree.

Table 4: Jointly optimized differentiated T' coefficients for the the Helmholtz resonator tree.

name	value	name	value	name	value
$T'_{C_{00}}$	21.20 µs	$T'_{C_{10}}$	19.95 µs	$T'_{C_{11}}$	20.35 µs
$T'_{L_{00}}$	34.80 µs	$T'_{L_{10}}$	24.79 µs	$T'_{L_{11}}$	25.10 µs

$$\boldsymbol{a}_e = \begin{bmatrix} -1 \\ 0 \\ 0 \\ 0 \\ 0 \\ 0 \\ 0 \end{bmatrix} \quad \text{and} \quad \mathbf{Z}_l = \operatorname{diag}\left(\begin{bmatrix} R_{00} \\ sL_{00} \\ 1/sC_{00} \\ R_{10} \\ sL_{10} \\ 1/sC_{10} \\ R_{11} \\ sL_{11} \\ 1/sC_{11} \end{bmatrix} \right). \quad (30)$$

We optimize the voltage–current response (i_0/e_0) of this system with the component values from Tab. 3. As designed, this system presents three distinct resonant peaks of similar intensity and quality factor, meaning three salient elements widely spread over the frequency range. Also, while the circuit may appear as three RLC series sub-circuits (highlighted with three different colors in Figs. 6 and 7), the parallel connections (denoted ∥ in Fig. 7) generate a load between those sub-circuits that prevents treating them independently, since the properties of each resonant peak are functions of all the components. Note also that since the frequency response exhibits multiple salient features, there is no longer a typical heuristic for the selection of a system-wide T' coefficient as it can only be tuned to a single frequency. For comparison, we find instead a system-wide coefficient $T' = 26.22\,\mu s$ for the parametric bilinear transform that minimizes the error ε.

Table 5: Error ε for the standard bilinear transform and the differentiated approach applied to the Helmholtz resonator tree.

	BLT	PBLT	Diff.
ε	14.7981	1.9538	0.3372

Tab. 4 shows the differentiated T' coefficients found after the joint optimization. Tab. 5 shows how the differentiated approach lowers the error by two orders of magnitude compared to the standard bilinear transform and one order of magnitude compared to the optimized parametric bilinear transform. Fig. 8 shows the frequency responses and error $|H_\Omega - \hat{H}_\Omega|$ for the standard bilinear transform, optimized parametric bilinear transform and the jointly optimized differentiated approach. The warping distortion of the standard bilinear transform introduces error, most significantly around the resonant peak with the highest frequency. Optimizing a system-wide parametrization of the parametric bilinear transform matches better that peak in frequency, but does not match its width or the frequency and width of the peaks at lower frequencies. By jointly optimizing differentiated T' coefficients, the error is distributed much more uniformly across the entire frequency range. We also get a very large error improvement around the resonant peak with the highest frequency and a discretized system frequency response that exhibits three resonant peaks with the correct frequency and width.

5 Conclusion and future work

In this paper, we introduce a new mathematical framework for the design of discretization schemes for linear circuits and sub-circuits in electronic audio effects. In

this approach, we differentiate the discretization coefficients among linear elements and jointly optimize them to improve the fit (i.e., minimize the error) between the frequency response of the original system and its discretized version.

Using the Tableau formulation of the circuit, we provide the analytical matrix expression of the system transfer function and frequency response error. This allows us to jointly optimize the different discretization coefficients for the case of linear circuits/sub-circuits with one free port without explicitly forming the full transfer function expression. We also present in more detail the case where each linear element is discretized using some form of the parametric bilinear transform (with differentiated parametrization across linear elements). This approach is successfully applied to two circuit examples, deriving jointly optimized differentiated parametrizations of the parametric bilinear transform applied to each element. In both cases, our approach significantly lowers the resulting frequency response error compared to typical approaches based on the standard and parametric bilinear transform.

Future work will extend the mathematical framework to wider classes of numerical methods, and study in greater depth other system structures of interest in linear (e.g., ladder circuits) and nonlinear audio circuits. We will also formulate alternative error functions, and explore solutions to improve the efficiency and robustness of their minimization (e.g., regularization).

References

[1] Moin, P., *Fundamentals of engineering numerical analysis*, Cambridge Univ. Press, New York, NY, 2010.

[2] Bilbao, S., *Numerical sound synthesis: Finite difference schemes and simulation in musical acoustics*, J. Wiley, Chichester, UK, 2009.

[3] Yeh, D., Abel, J., Vladimirescu, A., and Smith, J., "Numerical methods for simulation of guitar distortion circuits," *Comput. Music J.*, 32(2), p. 23–42, 2008.

[4] Al-Alaoui, M. A., "Novel stable higher order s-to-z transforms," *IEEE Trans. Circuits Syst. I, Fundam. Theory Appl.*, 48(11), p. 1326–9, 2001.

[5] Pei, S.-C. and Hsu, H.-J., "Fractional bilinear transform for analog-to-digital conversion," *IEEE Trans. Signal Process.*, 56(5), p. 2122–7, 2008.

[6] Rabiner, L. and Gold, B., *Theory and application of digital signal processing*, Prentice Hall, Englewood Cliffs, NJ, 1975.

[7] Al-Alaoui, M., "Al-Alaoui operator and the new transformation polynomials for discretization of analogue systems," *Elect. Eng.*, 90(6), p. 455–67, 2008.

[8] Stilson, T., *Efficiently-variable non-oversampled algorithms in virtual-analog music synthesis*, Ph.D. diss., Stanford Univ., 2006.

[9] Maestre, E., Scavone, G., and Smith, J., "Design of recursive digital filters in parallel form by linearly constrained pole optimization," *IEEE Signal Process. Lett.*, 23(11), p. 1547–50, 2016.

[10] Smith, J., *Physical audio signal processing*, W3K Pub., 2010.

[11] Yeh, D. T.-M., Abel, J. S., and Smith, J. O., "Automated physical modeling of nonlinear audio circuits for real-time audio effects—Part I: Theoretical development," *IEEE Trans. Audio, Speech, Language Process.*, 18(4), pp. 728–737, 2010.

[12] Holters, M. and Zölzer, U., "A Generalized Method for the Derivation of Non-Linear State-Space Models From Circuit Schematics," in *Proc. 23rd European Signal Process. Conf.*, Nice, France, 2015.

[13] Werner, K., Smith, J., and Abel, J., "Wave Digital Filter Adaptors for Arbitrary Topologies and Multiport Linear Elements," in *Proc. 18th Int. Conf. Digital Audio Effects*, Trondheim, Norway, 2015.

[14] Werner, K., Nangia, V., Smith, J., and Abel, J., "Resolving Wave Digital Filters with Multiple/Multiport Nonlinearities," in *Proc. 18th Int. Conf. Digital Audio Effects*, Trondheim, Norway, 2015.

[15] Smith, J., *Introduction to digital filters with audio applications*, W3K Pub., 2007.

[16] Germain, F. and Werner, K., "Design principles for lumped model discretisation using Möbius transforms," in *Proc. 18th Int. Conf. Digital Audio Effects*, Trondheim, Norway, 2015.

[17] Werner, K., Dunkel, W., and Germain, F., "A computational model of the Hammond organ vibrato/chorus using wave digital filters," in *Proc. 19th Int. Conf. Digital Audio Effects*, Brno, Czech Republic, 2016.

[18] Hu, F., Hussaini, M., and Manthey, J., "Low-dissipation and low-dispersion Runge–Kutta schemes for computational acoustics," *J. Comput. Phys.*, 124(1), p. 177–91, 1996.

[19] Bogey, C. and Bailly, C., "A family of low dispersive and low dissipative explicit schemes for flow and noise computations," *J. Comput. Phys.*, 194(1), p. 194–214, 2004.

[20] Hamilton, B. and Bilbao, S., "Fourth-order and optimised finite difference schemes for the 2-D wave equation," in *Proc. 16th Int. Conf. Digital Audio Effects*, Maynooth, Ireland, 2013.

[21] Holmes, B. and van Walstijn, M., "Physical model parameter optimisation for calibrated emulation of the Dallas Rangemaster Treble Booster guitar pedal," in *Proc. 19th Int. Conf. Digital Audio Effects*, Brno, Czech Republic, 2016.

[22] Werner, K., *Virtual Analog Modeling of Audio Circuitry Using Wave Digital Filters*, Ph.D. diss., Stanford University, Stanford, CA, USA, 2016.

[23] Van Valkenburg, M., *Introduction to modern network synthesis*, John Wiley & Sons, New York, NY, 1960.

[24] Fettweis, A., "Wave digital filters: Theory and practice," *Proc. IEEE*, 74(2), p. 270–327, 1986.

[25] Vlach, J. and Singhal, K., *Computer methods for circuit analysis and design*, van Nostrand Reinhold Company, New York, NY, 1983.

[26] Zhang, F., *The Schur complement and its applications*, Springer, New York, NY, 2005.

[27] Paiva, R. and Välimäki, V., "The Helmholtz resonator tree," in *Proc. 15th Int. Conf. Digital Audio Effects*, York, UK, 2012.

[28] Gander, W. and Gautschi, W., "Adaptive quadrature – revisited," *BIT*, 40, p. 84–101, 2000.

[29] Coleman, T. and Li, Y., "An interior, trust region approach for nonlinear minimization subject to bounds," *SIAM J. Optimiz.*, 6, p. 418–45, 1996.